SINTEF Energi AS
SINTEF Energy Research AS

Address:
Postboks 4761 Torgarden
7465 Trondheim
NORWAY

www.sintef.no

Enterprise Number:
NO 939 350 675 MVA

Project Memo

STAS Electric 1.0 – Theory Manual

VERSION
1.0

DATE
March 7, 2019

Author(s)
Karl Merz

CLIENT(S)
OPWIND

CLIENT'S REFERENCE
Part of D1.1.2

PROJECT
502001647

NUMBER OF PAGES AND ATTACHMENTS
12

ABSTRACT
This theory manual describes the equations implemented in Version 1.0 of the STAS Electric module. This generates nonlinear and linear state-space equations that describe the dynamics of the wind turbine electrical components, including the converters' active and reactive power controls. State-space models of transformers and cables are also included, such that a full wind power plant, including the collector grid and export cables, can be modelled.

PREPARED BY
Karl Merz

SIGNATURE

APPROVED BY
John Olav Tande

SIGNATURE

PROJECT MEMO NUMBER
AN 19.12.07

CLASSIFICATION
Unrestricted

Document History

VERSION	DATE	VERSION DESCRIPTION
1.0	06.09.2018	Original document

SINTEF

Contents

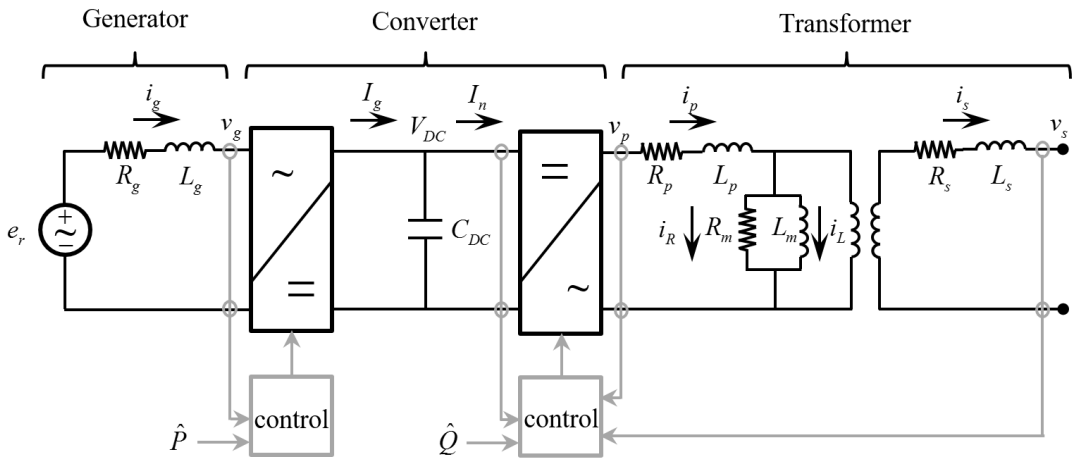

Figure 1: An equivalent circuit model of wind turbine electrical components.

1 Background

This theory manual describes the equations implemented in the STAS Electric module. The present Version 1.0 includes elementary equivalent-circuit models of turbine and grid electrical components, suitable for studies of power system dynamics and stability, below the fundamental AC frequency. The converter controls are given special consideration, as the hierarchy of measurements and feedback controls governs how rapidly the electrical system is able to respond to power set-point commands and disturbances.

Dynamic equations are implemented for the generator and transformer windings, as well as the DC link. Including the electrical dynamics in this way may not be strictly necessary; see Chapter 5 of Kundur (1994) for a discussion on this point. An alternative is to solve the electrical state equations for their steady-state values at each step, setting the left-hand-side time derivative to zero. That said, it is so that the timescales of the lowest levels of control are limited by the dynamics of the electrical components and sensor filtering; the next level of controls are limited by the first level; and so on, up to the turbine and even the plant levels. For many applications the lower-level dynamics can be simplified into an equivalent first-order filter; but by including the physical dynamic equations, we can confirm that the correct timescale is obtained, and also identify the lower-level problems that arise if one tries to increase the rate of response of the higher-level controls.

2 Governing equations

Figure 1 illustrates an equivalent circuit model of a wind turbine's electrical components. The governing equations are adapted from D'Arco *et al.* (2015) and Merz (2015). More information on the vector control strategy for converters can also be found in Anaya-Lara *et al.* (2009).

2.1 Generator

The generator is modelled as a voltage source acting through an impedance. The state equation is written in the *d-q* frame, with the *d* axis aligned with the magnetic North pole of the generator rotor. This gives

$$\mathbf{T}_a^\theta \mathbf{L}_g(I)\, \mathbf{T}_\theta^a \frac{d\mathbf{i}_g^\theta}{dt} = -\left(\omega_g \mathbf{T}_a^\theta \mathbf{L}_g(I)\, \frac{d\mathbf{T}_\theta^a}{d\theta} + \mathbf{T}_a^\theta \mathbf{R}_g\, \mathbf{T}_\theta^a\right) \mathbf{i}_g^\theta - \mathbf{v}_g^\theta - \omega_g \mathbf{T}_a^\theta \frac{d\mathbf{T}_\theta^a}{d\theta} \boldsymbol{\lambda}_r^\theta. \tag{1}$$

Quantities are defined in Fig. 1; also ω_g is the generator electrical speed,

$$\omega_g = \frac{n_p}{2}\Omega, \tag{2}$$

and

$$\boldsymbol{\lambda}_r^\theta = \mathbf{T}_a^\theta \begin{bmatrix} \lambda_{r,a} \\ \lambda_{r,b} \\ \lambda_{r,c} \end{bmatrix} = \begin{bmatrix} \lambda_r^\theta \\ 0 \end{bmatrix} \tag{3}$$

contains the rotor magnetic flux linking each phase. The d-q transform employed here is the power-equivalent version,

$$\mathbf{T}_a^\theta = \sqrt{\frac{2}{3}} \begin{bmatrix} \cos\theta & \cos(\theta - 2\pi/3) & \cos(\theta - 4\pi/3) \\ -\sin\theta & -\sin(\theta - 2\pi/3) & -\sin(\theta - 4\pi/3) \end{bmatrix}. \tag{4}$$

This means that the root-mean-square current or voltage is related to the d-q values by

$$I = \frac{1}{\sqrt{3}}\sqrt{(i_d^\theta)^2 + (i_q^\theta)^2}, \tag{5}$$

while the power is

$$P = (\mathbf{v}^\theta)^T \mathbf{i}^\theta. \tag{6}$$

In general, the phase inductance matrix $\mathbf{L}_g$ may be fully populated – that is, there is flux linkage hence mutual inductance between phases. It is often the case that the mutual inductance is negligible, and in this case

$$\mathbf{L}_g = \begin{bmatrix} L_g & 0 & 0 \\ 0 & L_g & 0 \\ 0 & 0 & L_g \end{bmatrix} = L_g \mathbf{I}. \tag{7}$$

Then,

$$\mathbf{T}_a^\theta \mathbf{L}_g \mathbf{T}_\theta^a = \begin{bmatrix} L_g & 0 \\ 0 & L_g \end{bmatrix}, \tag{8}$$

and similarly with $\mathbf{R}_g$;

$$\omega_g \mathbf{T}_a^\theta \mathbf{L}_g \frac{d\mathbf{T}_\theta^a}{d\theta} = \omega_g L_g \begin{bmatrix} 0 & -1 \\ 1 & 0 \end{bmatrix}; \tag{9}$$

and

$$\omega_g \mathbf{T}_a^\theta \frac{d\mathbf{T}_\theta^a}{d\theta} \boldsymbol{\lambda}_r^\theta = \omega_g \begin{bmatrix} 0 & -1 \\ 1 & 0 \end{bmatrix} \begin{bmatrix} \lambda_r^\theta \\ 0 \end{bmatrix} = \omega_g \begin{bmatrix} 0 \\ \lambda_r^\theta \end{bmatrix}. \tag{10}$$

Eq. (1) can be simplified to

$$L_g(I)\,\frac{d\mathbf{i}_g^\theta}{dt} = -\left(\omega_g L_g(I) \begin{bmatrix} 0 & -1 \\ 1 & 0 \end{bmatrix} + R_g\right) \mathbf{i}_g^\theta - \mathbf{v}_g^\theta - \omega_g \begin{bmatrix} 0 \\ \lambda_r^\theta \end{bmatrix}. \tag{11}$$

The core material of a generator may saturate magnetically during overcurrent events. As a result, the relationship between the terminal voltage and stator current is altered. The inductance becomes nonlinear, the waveforms exhibit harmonics, and high peak values of current may occur. Neglecting the harmonics, the effect of saturation on the fundamental frequency can be accounted for by an effective value of the inductance $L_g(I)$, which is specified as a function of the RMS current I. The inductance is nearly constant at low values of current, and decreases at high values of current, as the magnetic material saturates (Wijenayake and Schmidt 1997, Lovelace *et al.* 2002). In STAS Electric, the values of L_g are input for four values of I, and a spline is fit through these points.

The air-gap torque between the rotor and stator is

$$T_g = -\frac{1}{2} n_p \mathbf{T}_a^\theta \frac{d\mathbf{T}_\theta^a}{d\theta} \boldsymbol{\lambda}_r^\theta \cdot \mathbf{i}_g^\theta, \tag{12}$$

or in light of (10),

$$T_g = -\frac{1}{2} n_p \lambda_r^\theta (\mathbf{i}_g^\theta)_q. \tag{13}$$

2.2 Transformer

As seen in Fig. 1, the transformer is modelled with primary and secondary impedances, with a path representing the excitation branch. The equations for a single phase are then

$$\begin{bmatrix} L_p & 0 & L_m \\ 0 & aL_s & -L_m \\ 0 & 0 & L_m \end{bmatrix} \frac{d}{dt} \begin{bmatrix} i_p \\ i_s \\ i_L \end{bmatrix} = \begin{bmatrix} -R_p & 0 & 0 \\ 0 & -aR_s & 0 \\ R_m & -R_m/a & -R_m \end{bmatrix} \begin{bmatrix} i_p \\ i_s \\ i_L \end{bmatrix} + \begin{bmatrix} 1 & 0 \\ 0 & a \\ 0 & 0 \end{bmatrix} \begin{bmatrix} v_p \\ v_s \end{bmatrix}. \tag{14}$$

with $a = n_p/n_s$ being the turns ratio. The inclusion of the excitation branch in (14) can lead to poor numerical conditioning, and often has a negligible impact on the response over the frequency band and operating conditions of interest. Omitting the excitation branch, the equation for a single phase is simply

$$(L_p + a^2 L_s)\frac{di_p}{dt} = -(R_p + a^2 R_s)i_p + v_p - a v_s, \tag{15}$$

that is, an equivalent series impedance, here referenced to the primary side of the transformer. Considering all three phases, implementing the d-q transform, and explicitly writing the inductance as a function of the RMS current,

$$\mathbf{T}_a^\theta \mathbf{L}_t(I)\, \mathbf{T}_\theta^a \frac{d\mathbf{i}_p^\theta}{dt} = -\left(\omega_e \mathbf{T}_a^\theta \mathbf{L}_t(I)\, \frac{d\mathbf{T}_\theta^a}{d\theta} + \mathbf{T}_a^\theta \mathbf{R}_t\, \mathbf{T}_\theta^a\right) \mathbf{i}_p^\theta + \mathbf{v}_p^\theta - a\mathbf{v}_s^\theta. \tag{16}$$

Neglecting the mutual inductances in the manner of (7), (16) simplifies to

$$L_t(I)\, \frac{d\mathbf{i}_p^\theta}{dt} = -\left(\omega_e L_t(I) \begin{bmatrix} 0 & -1 \\ 1 & 0 \end{bmatrix} + R_t\right) \mathbf{i}_p^\theta + \mathbf{v}_p^\theta - a\mathbf{v}_s^\theta. \tag{17}$$

In STAS Electric the function $L_t(I)$ is defined by a spline curve fit through four input (I, L_t) points.

2.3 DC link and converters

The DC link dynamics are governed by the properties of its capacitor. The cables are short, so the resistance is neglected. The governing equation is

$$\frac{dV_{\mathrm{DC}}}{dt} = \frac{I_g - I_n}{C_{\mathrm{DC}}}. \tag{18}$$

Each converter is modelled as a black-box device that provides a controlled terminal voltage, while passing the active power to or from the DC link, with a small loss. On the rectifier (generator) side, the DC link current is[1]

$$I_g = \eta \frac{(\mathbf{v}_g^\theta)^T \mathbf{i}_g^\theta}{V_{\mathrm{DC}}}, \tag{19}$$

while on the inverter (network) side,

$$I_n = \frac{1}{\eta} \frac{(\mathbf{v}_p^\theta)^T \mathbf{i}_p^\theta}{V_{\mathrm{DC}}}. \tag{20}$$

[1] Should the generator for some reason be commanded to act as a motor, reversing the direction of power flow through the converters, then the efficiencies should be redefined as $\eta_{\mathrm{motor}} = 1/\eta_{\mathrm{gen}}$.

2.4 Control of the generator-side converter

The terminal voltage on the generator-side converter is controlled such that the current obtains a desired value. The current command comes from a higher-level control function that is based on the commanded active power, and perhaps also a function to damp oscillations of the driveshaft.[2]

Let there be a measurement of the electrical speed, say, from a rotor shaft encoder,

$$\frac{d\overline{\Omega}_g}{dt} = -\alpha_\Omega \overline{\Omega}_g + \alpha_\Omega \Omega_g, \qquad \overline{\omega}_g = \frac{N_p}{2}\overline{\Omega}_g, \tag{21}$$

where $\overline{\Omega}_g$ is the shaft speed and $\overline{\omega}_g$ is the electrical speed. A measurement of the generator terminal current $\mathbf{i}_g^\theta$ is also taken,

$$\frac{d\bar{\mathbf{i}}_g^\theta}{dt} = -\alpha_g \bar{\mathbf{i}}_g^\theta + \alpha_g \mathbf{i}_g^\theta. \tag{22}$$

Define the current error and its integral,

$$\boldsymbol{\varepsilon}_g = \hat{\mathbf{i}}_g^\theta - \bar{\mathbf{i}}_g^\theta, \qquad \frac{d\boldsymbol{\Psi}_g}{dt} = \mathbf{K}_{I,g}\boldsymbol{\varepsilon}_g. \tag{23}$$

The generator terminal voltage is controlled as

$$\mathbf{v}_g^\theta = -\overline{L}_g \left(\mathbf{K}_{P,g}\boldsymbol{\varepsilon}_g + \boldsymbol{\Psi}_g + \overline{\omega}_g \begin{bmatrix} 0 & -1 \\ 1 & 0 \end{bmatrix} \bar{\mathbf{i}}_g^\theta + K_{F,g}\overline{\omega}_g \tilde{\boldsymbol{\lambda}}_r^\theta \right), \tag{24}$$

where $\overline{L}_g$ is the estimated generator inductance, evaluated at the measured current amplitude $\overline{I}_g$. Substituting (24) into (11), the response of the generator current is

$$\frac{d\mathbf{i}_g^\theta}{dt} = \mathbf{K}_{P,g}\boldsymbol{\varepsilon}_g + \boldsymbol{\Psi}_g + \overline{\omega}_g \begin{bmatrix} 0 & -1 \\ 1 & 0 \end{bmatrix} \bar{\mathbf{i}}_g^\theta - \omega_g \begin{bmatrix} 0 & -1 \\ 1 & 0 \end{bmatrix} \mathbf{i}_g^\theta - \frac{R_g}{L_g}\mathbf{i}_g^\theta + \left(K_{F,g}\overline{\omega}_g - \omega_g\right), \tag{25}$$

or if the measured quantities are accurate, R_g/L_g is small, and $K_{F,g} = 1$,

$$\frac{d\mathbf{i}_g^\theta}{dt} \approx \mathbf{K}_{P,g}\boldsymbol{\varepsilon}_g + \boldsymbol{\Psi}_g, \tag{26}$$

which is a favorable control dynamic. Equation (24) is a form of feedback linearization, using a mathematical model to compensate, in the control signal, for the electrical dynamics of the generator. The measurement delays (21) and (22) are important, as these place limits on the gains in (24) and thereby the speed with which the voltage controller can react. Although the voltage controller acts quickly in relation to the relevant timescales of structural resonance and power commmand tracking, the limits on the speed of the voltage control in turn place limits on the speed of the higher-level active power control, and so on up the levels of the hierarchy.

[2] We choose here to draw the line between the electrical system and turbine control system at the level of the current command. The reason for this is that the tuning for the voltage controller is rather independent of the damping and power command tracking functions, whereas these higher-level control functions depend on the particulars of the rotor and driveshaft dynamics. Since using generator torque fluctuations to actively damp driveshaft and rotor oscillations is in conflict with perfect tracking of a commanded power, the tradeoff between these functions needs to be considered at the level of the wind turbine – that is, it should be part of the wind turbine's controller – and not at the lower level of the electrical components. Power command tracking control is documented in the STAS Control Theory Manual.

2.5 Grid frequency measurement

The grid frequency is measured using a phase-locked loop (PLL). This takes as input the *abc* voltage waveforms. In the software, it is assumed that the grid voltage is given in the *d*-*q* frame – the grid voltage at some location is likely to be used as the reference for the *d* axis – and that the grid frequency ω_e and its integral, the "electrical angle" θ_e, are known. For use in the PLL, the input voltage must be converted from the *d*-*q* to the *abc* frame, and then back to a d'-q' frame that is based on the estimated electrical angle $\overline{\theta}_e$. For the present purposes, this operation is modelled by first transforming the actual network voltage into the new frame,

$$(\mathbf{v}_s^\theta)' = \mathbf{T}_a^\theta(\overline{\theta}_e)\,\mathbf{T}_\theta^a(\theta_e)\,\mathbf{v}_s^\theta, \tag{27}$$

and then filtering the output to represent a measurement delay,

$$\frac{d\overline{\mathbf{v}}_s^\theta}{dt} = -\alpha_v \overline{\mathbf{v}}_s^\theta + \alpha_v (\mathbf{v}_s^\theta)'. \tag{28}$$

Note that

$$\mathbf{T}_a^\theta(\overline{\theta}_e)\,\mathbf{T}_\theta^a(\theta_e) = \begin{bmatrix} \cos\overline{\theta}_e\cos\theta_e + \sin\overline{\theta}_e\sin\theta_e & \sin\overline{\theta}_e\cos\theta_e - \cos\overline{\theta}_e\sin\theta_e \\ \cos\overline{\theta}_e\sin\theta_e - \sin\overline{\theta}_e\cos\theta_e & \cos\overline{\theta}_e\cos\theta_e + \sin\overline{\theta}_e\sin\theta_e \end{bmatrix} := \mathbf{T}_\delta. \tag{29}$$

A PI controller alters the measured frequency such that the phase of the measured voltage, in the *d*-*q* frame, is zero. This step consists of

$$\frac{d\Psi_e}{dt} = K_{I.e}\tan^{-1}\frac{(\overline{\mathbf{v}}_s^\theta)_q}{(\overline{\mathbf{v}}_s^\theta)_d} \tag{30}$$

and

$$\delta\overline{\omega}_e = K_{P,e}\tan^{-1}\frac{(\overline{\mathbf{v}}_s^\theta)_q}{(\overline{\mathbf{v}}_s^\theta)_d} + \Psi_e. \tag{31}$$

The measured frequency is then

$$\overline{\omega}_e = \delta\overline{\omega}_e + \hat{\omega}_e, \tag{32}$$

where $\hat{\omega}_e$ is a reference frequency.

2.6 Control of the network-side converter

The network-side converter controls the DC link voltage and reactive power, referred to the network-side terminals of the transformer. Unlike the generator-side converter, where the active power was relegated to a higher level of control, on the network side we consider the active power – which governs the DC link voltage – and reactive power control as part of the electrical system. It makes sense to organize things in this way, since the network-side converter control does not interact directly with any mechanical components.

Let the DC link voltage be measured,

$$\overline{V}_{\mathrm{DC}} = -\alpha_{\mathrm{DC}}\overline{V}_{\mathrm{DC}} + \alpha_{\mathrm{DC}}V_{\mathrm{DC}}; \tag{33}$$

and the current at the converter-side terminals of the transformer,

$$\frac{d\overline{\mathbf{i}}_p^\theta}{dt} = -\alpha_p\overline{\mathbf{i}}_p^\theta + \alpha_p\mathbf{i}_p^\theta; \tag{34}$$

also the current and voltage at the network-side terminals of the transformer, giving a measurement of the reactive power,

$$\overline{Q}_s = \overline{v}^{\theta}_{s,q}\overline{i}^{\theta}_{s,d} - \overline{v}^{\theta}_{s,d}\overline{i}^{\theta}_{s,q}, \qquad \frac{d\overline{\mathbf{i}}^{\theta}_s}{dt} = -\alpha_i\overline{\mathbf{i}}^{\theta}_s + \alpha_i\mathbf{i}^{\theta}_s, \qquad \frac{d\overline{\mathbf{v}}^{\theta}_s}{dt} = -\alpha_v\overline{\mathbf{v}}^{\theta}_s + \alpha_v\mathbf{v}^{\theta}_s, \tag{35}$$

The d-axis current is controlled in order to hold the DC link voltage at a reference value $\hat{V}_{\mathrm{DC}}$:

$$\varepsilon_{\mathrm{DC}} := \hat{V}_{\mathrm{DC}} - \overline{V}_{\mathrm{DC}}, \qquad \frac{d\Psi_{\mathrm{DC}}}{dt} = K_{I,\mathrm{DC}}\varepsilon_{\mathrm{DC}}, \tag{36}$$

$$\hat{i}^{\theta}_{p,d} = K_{P,\mathrm{DC}}\varepsilon_{\mathrm{DC}} + \Psi_{\mathrm{DC}}. \tag{37}$$

The q-axis current is controlled such that the commanded reactive power, referred to the network-side terminals of the transformer, is obtained:

$$\varepsilon_Q := \hat{Q}_s - \overline{Q}_s, \qquad \frac{d\Psi_Q}{dt} = K_{I,Q}\varepsilon_Q, \tag{38}$$

$$\hat{i}^{\theta}_{p,q} = K_{P,Q}\varepsilon_Q + \Psi_Q. \tag{39}$$

It is convenient to combine (37) and (39) as

$$\hat{\mathbf{i}}^{\theta}_p = \mathbf{K}_{P,n}\boldsymbol{\varepsilon}_n + \boldsymbol{\Psi}_n. \tag{40}$$

Define the current error and its integral,

$$\boldsymbol{\varepsilon}_p = \hat{\mathbf{i}}^{\theta}_p - \overline{\mathbf{i}}^{\theta}_p, \qquad \frac{d\boldsymbol{\Psi}_p}{dt} = \mathbf{K}_{I,p}\boldsymbol{\varepsilon}_p. \tag{41}$$

Then the converter is commanded to provide the voltage (which it is assumed to do, instantly)

$$\mathbf{v}^{\theta}_p = \overline{L}_t\left(\mathbf{K}_{P,p}\boldsymbol{\varepsilon}_p + \boldsymbol{\Psi}_p + \overline{\omega}_e\begin{bmatrix}0 & -1\\ 1 & 0\end{bmatrix}\overline{\mathbf{i}}^{\theta}_p + \mathbf{K}_{F,p}\overline{\mathbf{v}}^{\theta}_s\right). \tag{42}$$

This control strategy is similar to that of the generator-side converter, and the comments at the end of Section 2.4 apply here as well.

2.7 Electric cables

Each electrical cable is represented between terminals as a π-equivalent circuit, as sketched in Fig. 2. The state equation in the d-q frame is

$$\frac{d}{dt}\begin{bmatrix}\mathbf{i}^{\theta}_k\\ \mathbf{v}^{\theta}_k\end{bmatrix} = \begin{bmatrix}-\left(\frac{R}{L}\mathbf{I} + \omega_e\begin{bmatrix}0 & -1\\ 1 & 0\end{bmatrix}\right) & -\frac{1}{L}\mathbf{I}\\ \frac{1}{C}\mathbf{I} & -\omega_e\begin{bmatrix}0 & -1\\ 1 & 0\end{bmatrix}\end{bmatrix}\begin{bmatrix}\mathbf{i}^{\theta}_k\\ \mathbf{v}^{\theta}_k\end{bmatrix} + \begin{bmatrix}\mathbf{0} & \frac{1}{L}\mathbf{I}\\ -\frac{1}{C}\mathbf{I} & \mathbf{0}\end{bmatrix}\begin{bmatrix}\mathbf{i}^{\theta}_{k+1}\\ \mathbf{v}^{\theta}_{k-1}\end{bmatrix}. \tag{43}$$

For long transmission lines, a number of segments can be placed in series in order to better approximate the dynamic behavior.

3 Linearized equations

In developing these linearized equations, it is assumed that the gains in the converter controller are constant, not scheduled. Gain scheduling results in additional terms.

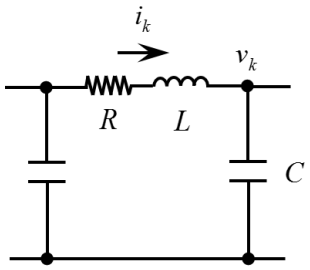

Figure 2: A π-equivalent circuit of an electrical cable.

3.1 Generator

For the simplified equation (11), we have

$$\begin{aligned} L_{g0}\frac{d\Delta\mathbf{i}_g^\theta}{dt} = &-\left(\omega_{g0}L_{g0}\begin{bmatrix}0 & -1\\ 1 & 0\end{bmatrix} + R_g + \frac{dL_g}{dI}\frac{\partial I}{\partial \mathbf{i}_g^\theta}\left.\frac{d\mathbf{i}_g^\theta}{dt}\right|_0 + \omega_{g0}\frac{dL_g}{dI}\frac{\partial I}{\partial \mathbf{i}_g^\theta}\begin{bmatrix}0 & -1\\ 1 & 0\end{bmatrix}\mathbf{i}_{g0}^\theta\right)\Delta\mathbf{i}_g^\theta \\ &- \Delta\mathbf{v}_g^\theta - \left(L_{g0}\begin{bmatrix}0 & -1\\ 1 & 0\end{bmatrix}\mathbf{i}_{g0}^\theta + \begin{bmatrix}0\\ \lambda_r^\theta\end{bmatrix}\right)\Delta\omega_g, \end{aligned} \tag{44}$$

where dL_g/dI comes from the saturation curve, and

$$\frac{\partial I}{\partial \mathbf{i}_g^\theta} = \frac{1}{\sqrt{3}\,I}(\mathbf{i}_g^\theta)^T. \tag{45}$$

3.2 Transformer

The linearized transformer dynamics are

$$\begin{aligned} L_{t0}\frac{d\Delta\mathbf{i}_p^\theta}{dt} = &-\left(\omega_{e0}L_{t0}\begin{bmatrix}0 & -1\\ 1 & 0\end{bmatrix} + R_t + \frac{dL_t}{dI_t}\frac{\partial I_t}{\partial \mathbf{i}_p^\theta}\left.\frac{d\mathbf{i}_p^\theta}{dt}\right|_0 + \omega_{e0}\frac{dL_t}{dI_t}\frac{\partial I_t}{\partial \mathbf{i}_p^\theta}\begin{bmatrix}0 & -1\\ 1 & 0\end{bmatrix}\mathbf{i}_{p0}^\theta\right)\Delta\mathbf{i}_p^\theta \\ &+ \Delta\mathbf{v}_p^\theta - a\Delta\mathbf{v}_s^\theta - L_{t0}\begin{bmatrix}0 & -1\\ 1 & 0\end{bmatrix}\mathbf{i}_{p0}^\theta\,\Delta\omega_e. \end{aligned} \tag{46}$$

3.3 DC link and converters

The capacitance of the DC link is considered to be constant, so (18) is already a linear equation,

$$\frac{d\Delta V_{\mathrm{DC}}}{dt} = \frac{1}{C_{\mathrm{DC}}}\Delta I_g - \frac{1}{C_{\mathrm{DC}}}\Delta I_n. \tag{47}$$

The expressions for the DC currents, however, are nonlinear, and are linearized as

$$\Delta I_g = \eta\frac{(\mathbf{v}_{g0}^\theta)^T}{V_{\mathrm{DC},0}}\Delta\mathbf{i}_g^\theta + \eta\frac{(\mathbf{i}_{g0}^\theta)^T}{V_{\mathrm{DC},0}}\Delta\mathbf{v}_g^\theta - \eta\frac{(\mathbf{v}_{g0}^\theta)^T(\mathbf{i}_{g0}^\theta)}{V_{\mathrm{DC},0}^2}\Delta V_{\mathrm{DC}} \tag{48}$$

and, similarly,

$$\Delta I_n = \frac{1}{\eta}\frac{(\mathbf{v}_{p0}^\theta)^T}{V_{\mathrm{DC},0}}\Delta\mathbf{i}_p^\theta + \frac{1}{\eta}\frac{(\mathbf{i}_{p0}^\theta)^T}{V_{\mathrm{DC},0}}\Delta\mathbf{v}_p^\theta - \frac{1}{\eta}\frac{(\mathbf{v}_{p0}^\theta)^T(\mathbf{i}_{p0}^\theta)}{V_{\mathrm{DC},0}^2}\Delta V_{\mathrm{DC}}. \tag{49}$$

3.4 Generator-side converter control

The control equations (21) through (23) are linear. The linearization of (24) is

$$\begin{aligned}\Delta\mathbf{v}_g^\theta = -\overline{L}_{g0}\left(\mathbf{K}_{P,g}\Delta\boldsymbol{\varepsilon}_g + \Delta\boldsymbol{\Psi}_g + \overline{\omega}_{g0}\begin{bmatrix}0 & -1\\ 1 & 0\end{bmatrix}\Delta\bar{\mathbf{i}}_g^\theta + \begin{bmatrix}0 & -1\\ 1 & 0\end{bmatrix}\bar{\mathbf{i}}_{g0}^\theta\Delta\overline{\omega}_g + K_{F,g}\tilde{\boldsymbol{\lambda}}_r^\theta\Delta\overline{\omega}_g\right)\\ - \left.\frac{\partial\overline{L}_g}{\partial\overline{I}}\right|_0\left.\frac{\partial\overline{I}}{\partial\bar{\mathbf{i}}_g^\theta}\right|_0\left(\mathbf{K}_{P,g}\boldsymbol{\varepsilon}_{g0} + \boldsymbol{\Psi}_{g0} + \overline{\omega}_{g0}\begin{bmatrix}0 & -1\\ 1 & 0\end{bmatrix}\bar{\mathbf{i}}_{g0}^\theta + K_{F,g}\overline{\omega}_{g0}\tilde{\boldsymbol{\lambda}}_r^\theta\right)\Delta\bar{\mathbf{i}}_g^\theta.\end{aligned} \tag{50}$$

3.5 Grid frequency measurement

Linearizing (27) gives

$$\Delta(\mathbf{v}_s^\theta)' = \mathbf{T}_\delta\,\Delta\mathbf{v}_s^\theta + \frac{\partial\mathbf{T}_\delta}{\partial\overline{\theta}_e}\mathbf{v}_{s0}^\theta\Delta\overline{\theta}_e + \frac{\partial\mathbf{T}_\delta}{\partial\theta_e}\mathbf{v}_{s0}^\theta\Delta\theta_e, \tag{51}$$

where

$$\frac{\partial\mathbf{T}_\delta}{\partial\theta_e} = \begin{bmatrix}-\cos\overline{\theta}_e\sin\theta_e + \sin\overline{\theta}_e\cos\theta_e & -\sin\overline{\theta}_e\sin\theta_e - \cos\overline{\theta}_e\cos\theta_e\\ \cos\overline{\theta}_e\cos\theta_e + \sin\overline{\theta}_e\sin\theta_e & -\cos\overline{\theta}_e\sin\theta_e + \sin\overline{\theta}_e\cos\theta_e\end{bmatrix} \tag{52}$$

and similarly for $\partial\mathbf{T}_\delta/\partial\overline{\theta}_e$. Then (28) is already linear,

$$\frac{d\Delta\overline{\mathbf{v}}_s^\theta}{dt} = -\alpha_v\,\Delta\overline{\mathbf{v}}_s^\theta + \alpha_v\,\Delta(\mathbf{v}_s^\theta)'. \tag{53}$$

Equations (30) and (31) are straightforward to linearize using

$$\frac{\partial}{\partial x}\tan^{-1}\frac{y}{x} = -\frac{y}{x^2+y^2} \quad\text{and}\quad \frac{\partial}{\partial y}\tan^{-1}\frac{y}{x} = \frac{x}{x^2+y^2}. \tag{54}$$

3.6 Network-side converter control

Equations (33) through (41) are linear, with the exception of

$$\Delta\overline{Q}_s = \begin{bmatrix}\overline{v}_{s,q0}^\theta & -\overline{v}_{s,d0}^\theta\end{bmatrix}\Delta\bar{\mathbf{i}}_s^\theta + \begin{bmatrix}-\bar{i}_{s,q0}^\theta & \bar{i}_{s,d0}^\theta\end{bmatrix}\Delta\overline{\mathbf{v}}_s^\theta. \tag{55}$$

Then, (42) is linearized as

$$\begin{aligned}\Delta\mathbf{v}_p^\theta = \overline{L}_{t0}\left(\mathbf{K}_{P,p}\Delta\boldsymbol{\varepsilon}_p + \Delta\boldsymbol{\Psi}_p + \overline{\omega}_{e0}\begin{bmatrix}0 & -1\\ 1 & 0\end{bmatrix}\Delta\bar{\mathbf{i}}_p^\theta + \begin{bmatrix}0 & -1\\ 1 & 0\end{bmatrix}\bar{\mathbf{i}}_{p0}^\theta\Delta\overline{\omega}_e + \mathbf{K}_{F,p}\Delta\overline{\mathbf{v}}_s^\theta\right)\\ + \left.\frac{\partial\overline{L}_t}{\partial\overline{I}}\right|_0\left.\frac{\partial\overline{I}}{\partial\bar{\mathbf{i}}_p^\theta}\right|_0\left(\mathbf{K}_{P,p}\boldsymbol{\varepsilon}_{p0} + \boldsymbol{\Psi}_{p0} + \overline{\omega}_{e0}\begin{bmatrix}0 & -1\\ 1 & 0\end{bmatrix}\bar{\mathbf{i}}_{p0}^\theta + \mathbf{K}_{F,p}\overline{\mathbf{v}}_{s0}^\theta\right)\Delta\bar{\mathbf{i}}_p^\theta.\end{aligned} \tag{56}$$

3.7 Electrical cables

The π-equivalent representation of a cable is linearized as

$$\frac{d}{dt}\begin{bmatrix}\Delta\mathbf{i}_k^\theta\\ \Delta\mathbf{v}_k^\theta\end{bmatrix} = \mathbf{A}_0\begin{bmatrix}\Delta\mathbf{i}_k^\theta\\ \Delta\mathbf{v}_k^\theta\end{bmatrix} + \mathbf{B}\begin{bmatrix}\Delta\mathbf{i}_{k+1}^\theta\\ \Delta\mathbf{v}_{k-1}^\theta\end{bmatrix} + \left.\frac{\partial\mathbf{A}}{\partial\omega_e}\right|_0\begin{bmatrix}\mathbf{i}_{k0}^\theta\\ \mathbf{v}_{k0}^\theta\end{bmatrix}\Delta\omega_e. \tag{57}$$

References

[1] Anaya-Lara O, *et al.* (2009). *Wind Energy Generation: Modelling and Control*. Wiley.

[2] Anaya-Lara O, *et al.* (2018). *Offshore Wind Energy Technology*. Wiley.

[3] D'Arco S, Suul JA, Fosso OB (2015). A virtual synchronous machine implementation for distributed control of power converters in SmartGrids. Electric Power Systems Research 122: 180-197.

[4] Kundur P (1994). *Power System Stability and Control*. McGraw-Hill.

[5] Lovelace EC, Jahns TM, Lang JH (2002). A saturating lumped-parameter model for an interior PM synchronous machine. IEEE Transactions on Industry Applications 38: 645-650.

[6] Merz KO (2015). Pitch actuator and generator models for wind turbine control system studies. Memo AN 15.12.35, SINTEF Energy Research.

[7] Wijenayake AH, Schmidt PB (1997). Modeling and analysis of permanent magnet synchronous motor by taking saturation and core loss into account. Proceedings of the Second International Conference on Power Electronics and Drive Systems, Singapore, May 26-29, 1997.

Technology for a better society

www.sintef.no